# IN SITU RAMAN SPECTROSCOPY OF SINGLE MICROPARTICLE $Li^+$-INTERCALATION ELECTRODES

Kaoru Dokko, Qingfang Shi, Ionel C. Stefan and Daniel A. Scherson
Department of Chemistry
Case Western Reserve University
Cleveland, OH 44106-7078

## ABSTRACT

Modifications in the vibrational properties of a single microparticle of $LiMn_2O_4$ induced by extraction and subsequent injection of $Li^+$ into the lattice have been monitored *in situ* via *simultaneous* acquisition of Raman scattering spectra and cyclic voltammetry data in 1M $LiClO_4$ solutions in ethylene carbonate (EC):diethyl carbonate (DEC) mixtures (1:1 by volume). Statistical analyses of the spectra in the range $15 < SOD < 45$ %, where SOD represents the state of discharge (in percent) of the nominally fully charged material, i.e. $\lambda$-$MnO_2$, were found to be consistent with the coexistence of two distinct phases of lithiated metal oxide in agreement with information derived from *in situ* X-ray diffraction (XRD) measurements involving more conventional battery-type electrodes (T. Eriksson, et al. *J. Electrochem. Soc.* **2002**, *149*, A69).

## INTRODUCTION

The development of *in situ* techniques for the characterization of the intrinsic properties of charge storage materials is expected to play a key role toward elucidating the factors that control important aspects of battery electrodes, including structural changes induced by charge and discharge, as well as capacity fade effects upon repeated cycling. Efforts are being made in several laboratories to eliminate possible interferences derived from the presence of additives, such as conductivity enhancers and binders, which may compromise reliable quantitative data analyses. Indeed, several schemes have been described in the literature for performing measurements on pure charge storage materials supported on inert conducting substrates, either as

films[1-7] or as single, [8-10,11] or ensembles of particles,[12-16] of the same type as those used in commercial devices. Particularly noteworthy is the work of Uchida and coworkers involving electrochemical measurements on single particle electrodes,[8-11] as well as that of our group at CWRU, which relies on the mechanical embedding of technical microparticles on either gold or nickel supports to examine *in situ* vibrational,[13,12,16] and electronic and structural properties [17,14] of $Li^+$-insertion electrodes as a function of their state of charge. Although important information has been derived from the analysis of results obtained from such experiments, it has not been possible so far to perform *simultaneously* spectroscopic and electrochemical measurements on single particle electrodes. This paper describes a novel experimental strategy that enables *in situ* Raman spectra of a single microparticle to be acquired while recording cyclic voltammograms at low scan rates, using $LiMn_2O_4$ in a $Li^+$-containing organic electrolyte as a model system. Key to the success of these experiments was the combined use of a microelectrode to both contact electrically and press mechanically the microparticle against an optical window, an airtight spectroelectrochemical cell, and a Raman microscope to focus the exciting laser radiation directly on the surface of the microparticle, while collecting the scattered light by the same objective lens.

**EXPERIMENTAL**

A schematic diagram of the all-glass, airtight, spectroelectrochemical cell, as well as of the overall experimental arrangement for *in situ* Raman spectroscopy of single particle microelectrodes is depicted in Panel A, Fig. 1. As indicated therein, the cell is equipped with a sapphire window (Esco Products Inc., 0.5 mm thick) sealed against the cell body with an O-ring (KALREZ®) using a metal clamp, and with a Li metal foil (2 $cm^2$) pressed against a tungsten wire as a counter/reference electrode. Electrical contact to the microparticle was achieved with a Pt microelectrode prepared by sealing the tip of a Pt wire (50 μm in diameter) into a Pyrex glass tube

using a hydrogen flame, which was later polished with sandpaper (CARBIMET®, GRIT 600) to expose a circularly shaped electrode. The other end of the Pt wire was attached to a much thicker Cu wire, which was used in turn as an external electrical contact. Prior to cell assembly, the microelectrode was pushed against the sapphire window and fixed firmly in that position using a Teflon bushing. The window was then detached from the cell, and a single $LiMn_2O_4$ particle (*ca.* 25 μm in diameter) placed in the center of the microelectrode (see Panel B, Fig. 1) utilizing the tip of a sharp needle as a manipulator under a conventional optical microscope. The window was once again mounted onto the cell body pressing the particle against the surface of the Pt disk with high enough force to keep it rigidly in position without compromising its integrity. At this stage, the cell was transferred to a glovebox (Vacuum Atmospheres) equipped with water and oxygen sensors, where it was later filled with a 1M $LiClO_4$ solution in a mixture of ethylene carbonate (EC) and diethyl carbonate (DEC) (1:1 by volume). Once carefully sealed, the cell was removed from the glove box and placed directly beneath the microscope objective of the Raman microscope (see below).

Raman spectra were acquired using a Raman 2000 system (Chromex Inc., Albuquerque, NM) equipped with a microscope attachment, using the same optical setup described elsewhere.[12] A focused (20X Olympus microscope) 532 nm laser beam (Verdi, Coherent) impinging onto the $LiMn_2O_4$ particle at near normal incidence (beam spot size on the particle *ca.* 5 μm diameter, see Panel B, Fig. 1), was used as the excitation source at powers low enough to avoid photothermal damage, and the scattered light was collected by the microscope objective. A Super-Notch-Plus filter (Kaiser Optical Systems, Inc., Ann Arbor, MI) placed just before the spectrograph stage was used to remove the primary beam. All data were obtained with the slit width set at 50 μm, with a spectral resolution of 2 $cm^{-1}$. A forced air-cooled charge coupled device (CCD) camera with 1024

× 256 pixels (Photometrics, Roper Scientific, Tucson, AZ) was employed as a detector. The integration time for each frame was 15 s with four frames co-added to improve the signal to noise ratio. Spectral contributions due to the sapphire window and the electrolyte were subtracted using commercial software (Origin). The electrode potential was controlled with a conventional potentiostat (AFRDE5, Pine Instruments), and all measurements were carried out at room temperature. Two complete cyclic voltammograms in the potential range $3.60 < E < 4.40$ V vs $Li/Li^+$ were recorded at a scan rate $\nu = 0.5$ mV/s for each particle with the cell placed under the Raman microscope prior to the spectroelectrochemical experiments. *In situ* Raman spectra were recorded continuously starting with the third cycle, while scanning the potential linearly at $\nu =$ 0.11 mV/s between the two prescribed values. Spectra were collected and coadded over a 60 s interval to yield signals averaged over a potential range of ca. 7 mV, and then stored for further processing. Statistical treatment of these data was performed using routines available in WinXAFS, an extended X-ray absorption fine structure analysis package.

**RESULTS AND DISCUSSION**

The (third) cyclic voltammogram (CV) of a single $LiMn_2O_4$ particle recorded at $\nu = 0.11$ mV/s in the spectroelectrochemical cell *during* acquisition of Raman spectra displayed two clearly defined sets of complementary peaks centered at around 4.0 (A/A') and 4.1 V (B/B') vs $Li/Li^+$ (see Fig. 2) in excellent agreement with data published elsewhere.[9] As has also been discussed thoroughly in the literature,[18] the charge under each of these peaks corresponds to about half the total amount of $Li^+$ in $LiMn_2O_4$ to form, in sequence, $Li_{0.5}Mn_2O_4$ and $\lambda$-$MnO_2$. The differences in the values of the peak potentials between complementary features observed in the scan in the positive and negative directions (Fig. 2) are somewhat smaller than those reported earlier by Luo *et al.* in our laboratory,[13] indicating that the iR drop in the present configuration is far reduced

despite the fact that the single particle electrode is actually touching the window. Also responsible for at least part of the hysteresis is the very small diffusion coefficient of $Li^+$ within the metal oxide lattice, which renders the system under partial (solid state) mass transport control even at the slow scan rate employed for these experiments. In view of the rather weak Raman signals observed between 3.6 and 4.0 V (not shown here), the laser was turned off while scanning within this range to avoid unnecessary heating of the particle. The slight changes in the current observed upon turning the laser on and off (see Fig. 2) are due to photoexcitation processes.

*In situ* potential-averaged Raman spectra acquired *continuously* during that third linear scan in the negative, and subsequent positive directions are shown in the upper (A, B, C) and lower panels (D, E, F) in Fig. 3, respectively, where the numbers on the right of each of the traces represent the average potential during spectral collection. As has been noted by other workers, the Raman features of $LiMn_2O_4$ are of much weaker intensities than those of $Li_{0.5}Mn_2O_4$ or the nominally fully delithiated material, $\lambda$-$MnO_2$; hence, no attempt was made to analyze data in the potential range $E < 4.021$ V vs $Li/Li^+$. Although lacking much resolution, the broad, and markedly asymmetric feature centered at ca. 600 $cm^{-1}$ found for $4.021 < E < 4.118$ V can be ascribed to two $T_2$ and two $A_1$ modes of $Li_{0.5}Mn_2O_4$. Two prominent peaks centered at 495, and particularly at 588 $cm^{-1}$, attributed to the $T_{2g}(2)$ and $A_{1g}$ modes of $\lambda$-$MnO_2$, respectively, could be discerned in the spectra collected for $E > 4.131$ V (see Panels A and B, Fig. 3). Quantum mechanical calculations[19] predict additional Raman active bands for this specific material at 479 $cm^{-1}$, $E_g$, and 630 $cm^{-1}$, $T_{2g}(3)$. Although both of these modes have been observed by other workers[19,20] (at i.e. 463 and 647 $cm^{-1}$, respectively), their presence could not be clearly identified in our *in situ* spectra owing probably to their lower Raman scattering cross sections. The increase in scattering intensity in the region of 450-700 $cm^{-1}$ for $E > 4.172$ V (up to 4.29 V, see Panel C) is due to resonance

enhancement effects associated with $\lambda$-$MnO_2$ at the excitation wavelength employed in these experiments.[19] A similar overall trend was found for spectra recorded during charging, as shown in Panels D through F in Fig. 3.

At least three factors must be considered before a quantitative analysis of the data collected can be pursued:

i. According to reports published in the literature,[21] the theoretical capacity of $LiMn_2O_4$ exceeds by about 20% the values found experimentally implying that a rather significant fraction of $Li^+$ is retained by the lattice even when the material is nominally fully charged.

ii. The total charge storage capacity of the microparticle examined, as measured via integration of the current in the scan in the positive direction, yielded a value of ca. 23.7 $\mu$C (see Panel A, Fig. 4) and thus ca. 10% smaller compared to the total charge released determined by a similar coulometric analysis of the subsequent scan in the negative direction. Such imbalance is mostly likely derived from oxidative solvent decomposition, an irreversible process that generates an additional charge contribution in the integrated scan in the positive direction.

iii. The scan rate employed in our studies ($\nu$ = 0.11 mV/s) was higher than that required for the microparticle to achieve full equilibration at any given potential, leading to slight distortions in the charge vs potential curves. In fact, even under these less than optimum conditions, a complete set of spectroelectrochemical measurements, (i.e. spectral acquisition during a full voltammetric cycle) took in excess of 4 h. It must be stressed, however, that in view of the small diffusion coefficient of $Li^+$ within the metal oxide lattice, and the rather small penetration depth of the beam, the spectral measurements are expected to represent rather accurately those of a particle in equilibrium with the applied potential.

For analysis to follow, it will be assumed that the state of discharge (SOD in %) of the electrode is defined as zero when the microparticle is polarized at the most positive potential, i.e. E = 4.30 V, and that its full capacity (one $Li^+$ per electron) corresponds to the charge released upon full nominal discharge (integration of the voltammetric curve down to E = 3.60 V). On this basis, it becomes possible to construct plots of SOD as a function of E, as shown in Panel B, Fig. 4, and to correlate these data with information derived from the spectroscopic measurements recorded *simultaneously*.

Of particular relevance to this study are the *in situ* X-ray diffraction (XRD) measurements reported by Eriksson et al.[22] for $Li_xMn_2O_4$, which are consistent with the presence of one single phase, denoted as 1, over the range 0 < SOD < 11 % (Phase 1) and a different single phase (2) over 35 < SOD < 100 %. Evidence was also obtained by these workers for the coexistence these two phases in the intermediate range 11 < SOD < 35 %, for which their respective lattice parameters remained fixed at 8.805 Å (Phase 1) and 8.145 Å (Phase 2). As shown in Panel A, Fig. 3, large drops in intensity were found in the Raman spectra recorded during the initial stages of discharge of the fully charged microparticle in which the only phase present (Phase 1) undergoes a linear lattice expansion as a function of the SOD. This behavior is in all likelihood related to changes in the electronic properties of the material as $Li^+$ is injected into the lattice, leading to a rapid loss of resonantly enhanced intensity associated with $\lambda$-$MnO_2$, a phenomenon that complicates a more quantitative interpretation of spectra recorded in this SOD region.

More amenable to a rigorous analysis, however, are spectral data acquired in the intermediate SOD range, where, as stated above, the lattice parameters of the two phases are independent of the SOD. To this end, the Raman spectra collected at SOD = ca. 16% and ca. 43%

were assumed to represent the pure phases 1 and 2, respectively, and *no restrictions were imposed while fitting the data on the sum of the constituent phases for each SOD*. Spectra used for analysis are indicated by thicker lines and pure phases by a star in panels B and E, Figure 3. Two typical examples of fits to the spectra are shown in Panels A and B, Fig. 6, which display both the contributions made by each of the two pure phases (Phase 1 as dashed line and Phase 2 as dotted line), as well as their sum (see continuous line superimposed on the scattered experimental points), for spectra recorded during the positive scan at 4.151 V (Panel A) and the negative scan at 4.097 V (Panel B). The values indicated in each of the curves represent the percent of each of the phases in the specimen as determined from the mathematical analysis. In analogy with the conclusions made by Eriksson et al.[22] based on their *in situ* XRD studies, the results derived from the statistical treatment of the Raman data for the microparticle yielded good linear correlations ($R > 0.99$) between the amount of each constituent phase and the SOD (see Fig. 5). Furthermore, the *unrestricted* sum of the components correctly predicts (within 2%) values very close to 1, lending strong support to the validity of the method implemented.

## CONCLUSIONS

Simultaneous *in situ* Raman spectroscopic and electrochemical measurements of a $LiMn_2O_4$ single particle (25 μm diameter) attached to a Pt micro-disk were successfully performed using a Raman microscope and a specially designed spectroelectrochemical cell. Statistical analysis of the data obtained yielded results consistent with information derived from XRD making it possible to correlate optical data with phase composition for SOD values in the range 11 and 35. Slight modifications to the methods described will make it possible to extend measurements of the type herein presented to a wide variety of energy storage materials, including graphite. The results emerging from such measurements will allow direct correlations to be made

between the state of charge of single particle electrodes and their Raman spectroscopic properties, thereby providing means of monitoring spatio-temporal effects induced by intercalation electrodes of interest to the operation and performance of energy storage devices.

**ACKNOWLEDGEMENTS**

This work was supported in part by NASA-Glenn and the US Department of Energy, Office of Basic Energy Sciences. Additional funding was provided by Eveready Battery Company, Westlake, OH. K.D may wish to express his deep appreciation to Prof. Isamu Uchida (Tohoku University) for his helpful comments. K.D. acknowledges a research fellowship from the Japan Society for the Promotion of Science.

**REFERENCES**

(1) Anzue, N.; Itoh, T.; Mohamedi, M.; Umeda, M.; Uchida, I. *Solid State Ionics* **2003**, *156*, 301-307.

(2) Desilvestro, J.; Corrigan, D. A.; Weaver, M. J. *J. Phys. Chem.* **1986**, *90*, 6408-6411.

(3) Desilvestro, J.; Corrigan, D. A.; Weaver, M. J. *J. Electrochem. Soc.* **1988**, *135*, 885-892.

(4) Dokko, K.; Mohamedi, M.; Anzue, N.; Itoh, T.; Uchida, I. *J. Mater. Chem.* **2002**, *12*, 3688-3693.

(5) Yamamura, S.; Koshika, H.; Nishizawa, M.; Matsue, T.; Uchida, I. *J. Solid State Electrochem.* **1998**, *2*, 211-215.

(6) Nishizawa, M.; Ise, T.; Koshika, H.; Itoh, T.; Uchida, I. *Chem. Mat.* **2000**, *12*, 1367-1371.

(7) Mohamedi, M.; Takahashi, D.; Uchiyama, T.; Itoh, T.; Nishizawa, M.; Uchida, I. *J. Power Sources* **2001**, *93*, 93-103.

(8) Dokko, K.; Horikoshi, S.; Itoh, T.; Nishizawa, M.; Mohamedi, M.; Uchida, I. *J. Power Sources* **2000**, *90*, 109-115.

(9) Dokko, K.; Nishizawa, M.; Mohamedi, M.; Umeda, M.; Uchida, I.; Akimoto, J.; Takahashi, Y.; Gotoh, Y.; Mizuta, S. *Electrochem. Solid State Lett.* **2001**, *4*, A151-A153.

(10) Dokko, K.; Mohamedi, M.; Umeda, M.; Uchida, I. *J. Electrochem. Soc.* **2003**, *150*, A425-A429

(11) Uchida, I.; Mohamedi, M.; Dokko, K.; Nishizawa, M.; Itoh, T.; Umeda, M. *J. Power Sources* **2001**, *97-8*, 518-524.

(12) Luo, Y.; Cai, W. B.; Scherson, D. A. *J. Electrochem. Soc.* **2002**, *149*, A1100-A1105.

(13) Luo, Y.; Cai, W.-B.; Scherson, D. A. *Electrochem. Solid State Lett.* **2001**, *4*, A101-A104.

(14) Totir, D. A.; Bae, I. T.; Hu, Y. N.; Antonio, M. R.; Stan, M. A.; Scherson, D. A. *J. Phys. Chem. B* **1997**, *101*, 9751-9756.

(15) Totir, D. A.; Cahan, B. D.; Scherson, D. A. *Electrochim. Acta* **1999**, *45*, 161-166.

(16) Totir, D. A.; Scherson, D. A. *Electrochem. Solid State Lett.* **2000**, *3*, 263-265.

(17) Totir, D. A.; Antonio, M. R.; Schilling, P.; Tittsworth, R.; Scherson, D. A. *Electrochim. Acta* **2002**, *47*, 3195-3200.

(18) Gao, Y.; Reimers, J. N.; Dahn, J. R. *Phys. Rev. B* **1996**, *54*, 3878-3883.

(19) Ammundsen, B.; Burns, G. R.; Islam, M. S.; Kanoh, H.; Roziere, J. *J. Phys. Chem. B* **1999**, *103*, 5175-5180.

(20) Kanoh, H.; Tang, W. P.; Ooi, K. *Electrochem. Solid State Lett.* **1998**, *1*, 17-19.

(21) Thackeray, M. M. *Prog. Solid State Chem.* **1997**, *25*, 1-71.

(22) Eriksson, T.; Andersson, A. M.; Bishop, A. G.; Gejke, C.; Gustafsson, T.; Thomas, J. O. *J. Electrochem. Soc.* **2002**, *149*, A69-A78.

## FIGURE CAPTIONS

**Figure 1.** Schematic diagram of the spectroelectrochemical cell employed in these studies for the acquisition of simultaneous *in situ* Raman and cyclic voltammetric measurements of a single particle microelectrode (Panel A). Shown in Panel B in this figure is a photograph acquired with the microscope attachment of the small area of the microelectrode including the Pt electrode the $LiMn_2O_4$ microparticle and the surrounding glass casing.

**Figure 2.** Third cyclic voltammogram (CV) of a single $LiMn_2O_4$ microparticle recorded at a scan rate of 0.11 mV/s (see text for details) in a 1M $LiClO_4$ solution in a mixture of ethylene carbonate (EC) and diethyl carbonate (DEC) (1:1 by volume) in the spectroelectrochemical cell *during* acquisition of Raman spectra. The exciting focused laser beam was turn ON and OFF at the points specified in the cyclic voltammogram.

**Figure 3.** Series of Raman spectra recorded while acquiring the cyclic voltammetry data for the single $LiMn_2O_4$ microparticle shown in Fig. 2 for the scan in the negative (Panels A-C) and positive (Panels D-F) directions. The average potential, E, during each spectral collection is indicated on the right, whereas selected values of the state of discharge (SOD, %) are shown on the left side of the curves. The spectra in thicker lines were used for quantitative analyses of phase composition (see Fig. 5).

**Figure 4.** Plots of Charge vs Potential (E) (Panel A) and State of Discharge (SOD) vs. E (Panel B) based on coulometric analyses of the cyclic voltammetric data in Fig. 2.

**Figure 5.** Plots of the fraction of the spectral component for Phase 1 (solid symbols) and Phase (open symbols) for data collected during the scan in the negative (circles) and positive (squares) scans based on a statistical analysis of the spectra shown in thick lines in Fig. 3. The sum of the contributions of each of the two spectrally determined phases to the total Raman spectra was 1 ±

0.02, whereas the linear fits to the data yielded R values larger than 99%.

**Figure 6**. Detailed statistical fits (see solid line through to the actual experimental Raman spectra in scattered points in the upper curves in each Panel) to the Raman data collected at 4.151 V during the positive scan (Panel A) and 4.097 V during the negative scan (Panel B). The bottom curves in each of the panels represent *to scale* the individual contributions from the two pure phases, i.e. SOD = 16 % (E = 4.166 V) for Phase 1, and SOD = 45 % (E = 4.126 V) for Phase 2 in Panel A, and SOD = 16 % (E = 4.118) V for Phase 1, and SOD = 43 % (E = 4.077 V) for Phase 2 in Panel B. The values adjacent to each of the lower curves in Panels A and B correspond to the best-fit percents of each of the phases at the specified potential.

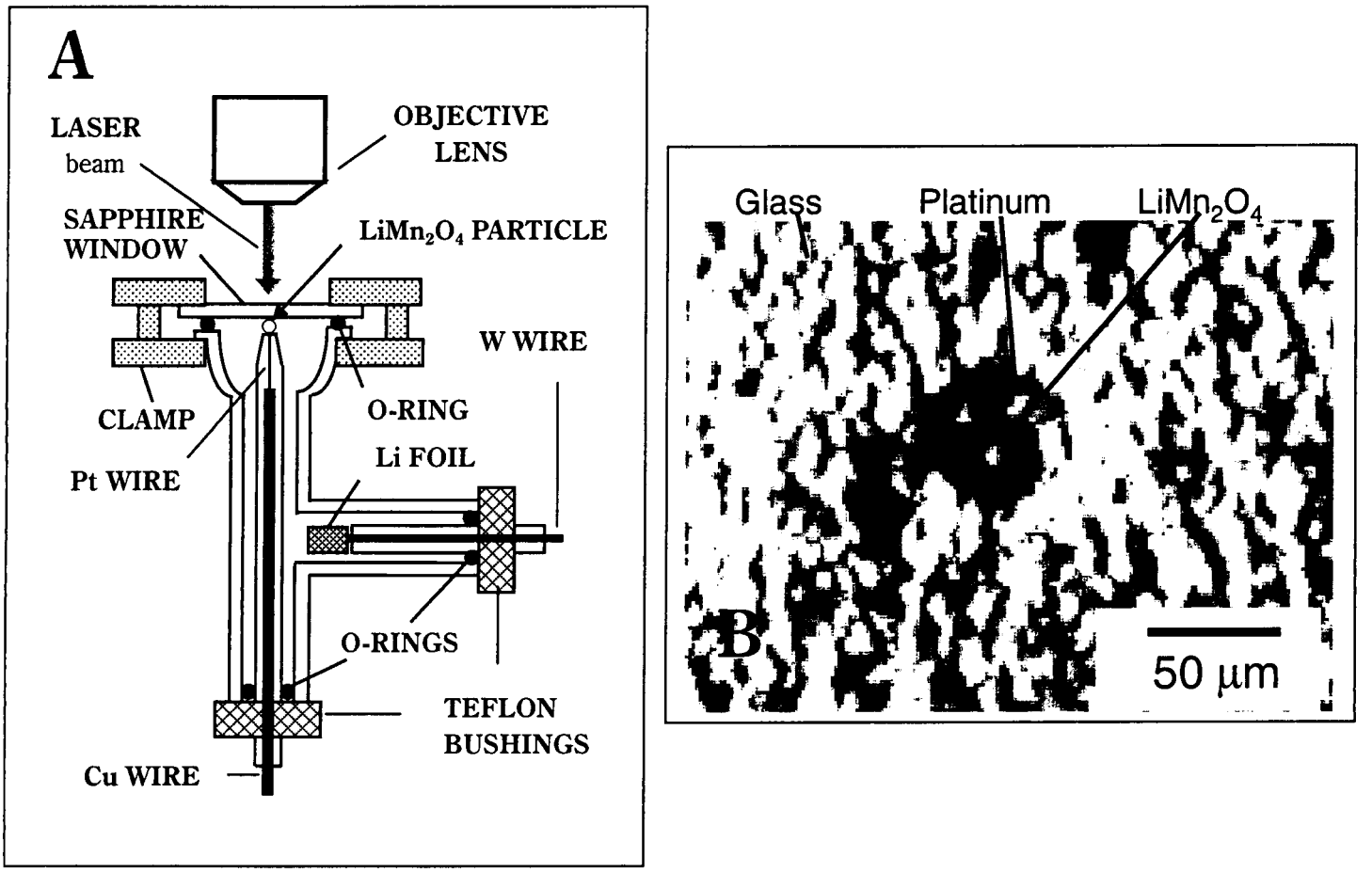


Figure 1. Schematic diagram of the spectroelectrochemical cell employed in these studies for the acquisition of simultaneous *in situ* Raman and cyclic voltammetric measurements of a single particle microelectrode (Panel A). Shown in Panel B in this figure is a photograph acquired with the microscope attachment of the small area of the microelectrode including the Pt electrode the $LiMn_2O_4$ microparticle and the surrounding glass casing.

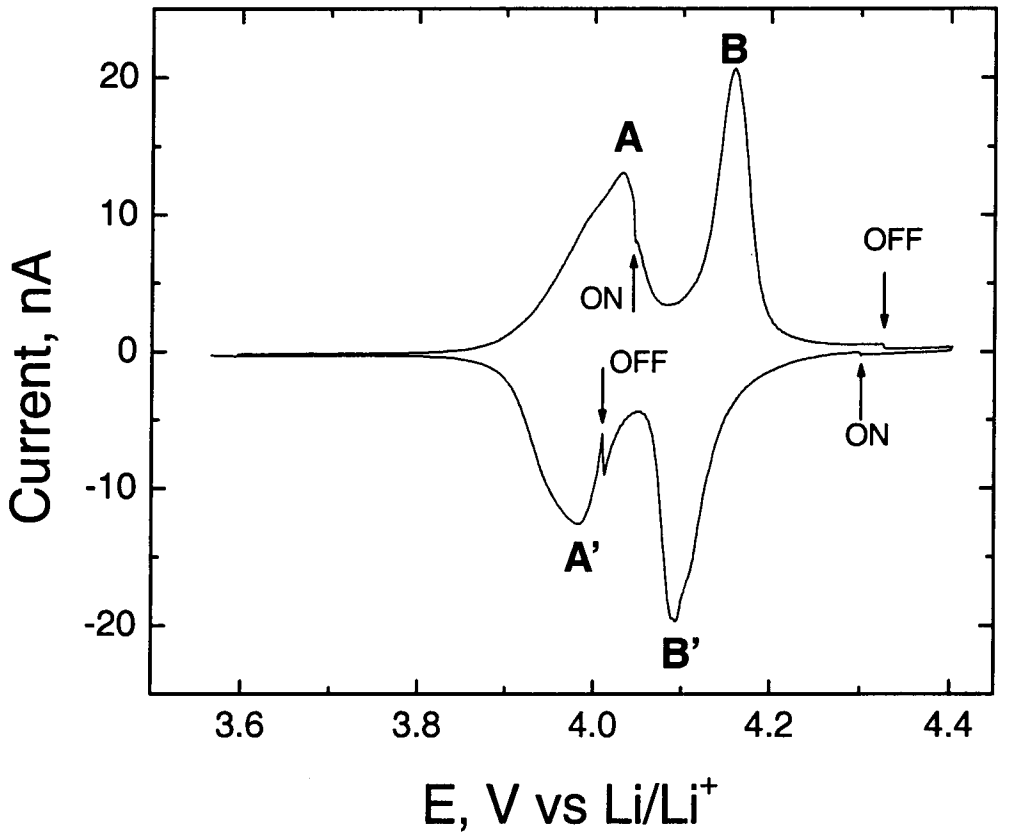


Figure 2. Third cyclic voltammogram (CV) of a single $LiMn_2O_4$ microparticle recorded at a scan rate of 0.11 mV/s (see text for details) in a 1M $LiClO_4$ solution in a mixture of ethylene carbonate (EC) and diethyl carbonate (DEC) (1:1 by volume) in the spectroelectrochemical cell *during* acquisition of Raman spectra. The exciting focused laser beam was turn ON and OFF at the points specified in the cyclic voltmmogram.

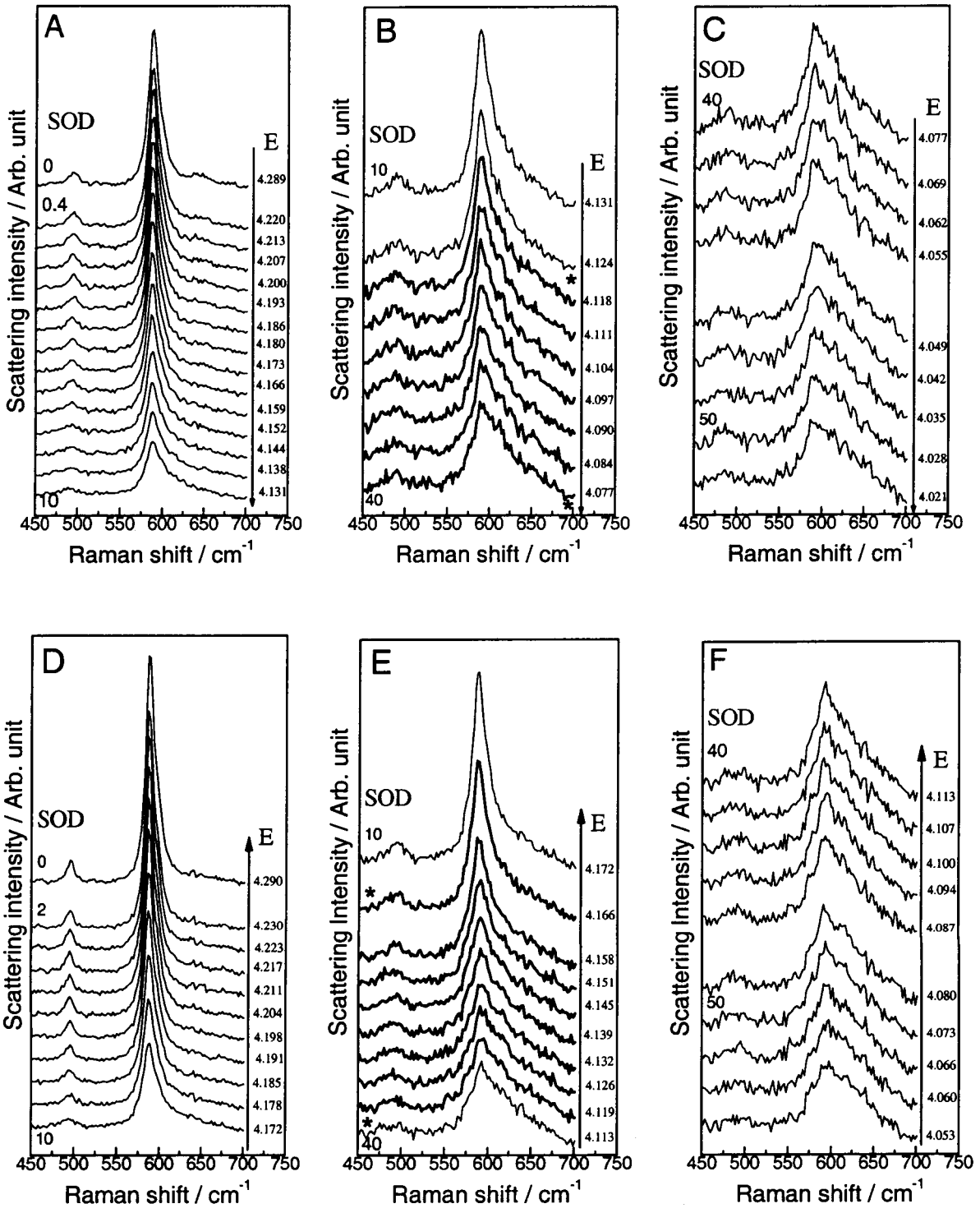


Figure 3. Series of Raman spectra recorded while acquiring the cyclic voltammetry data for the single $LiMn_2O_4$ microparticle shown in Fig. 2 for the scan in the negative (Panels A-C) and positive (Panels D-F) directions. The average potential, E , during each spectral collection is indicated on the right, whereas selected values of the state of discharge (SOD, %) are shown on the left side of the curves. The spectra in thicker lines were used for quantitative analyses of phase composition (see Fig. 5).

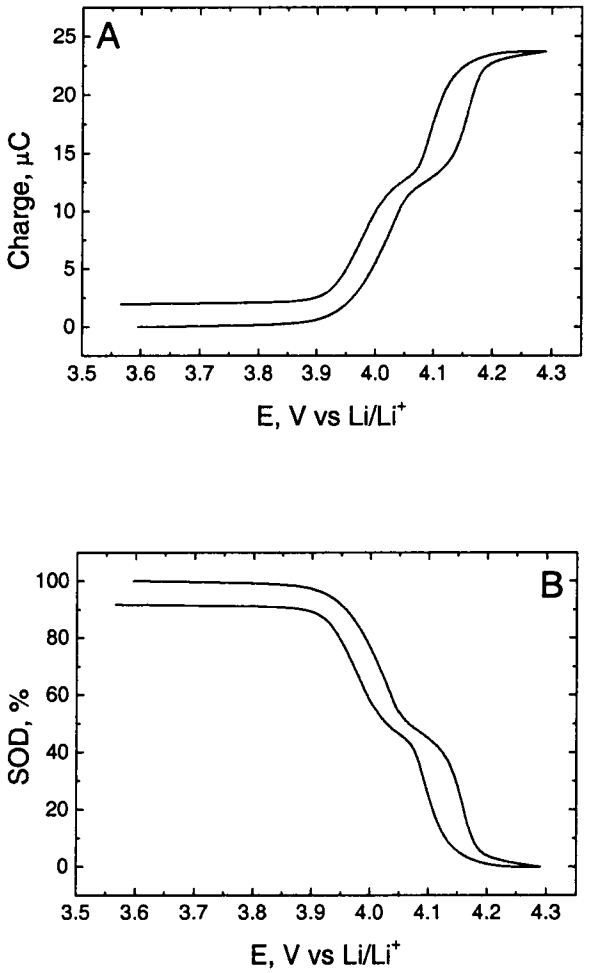


Figure 4. Plots of Charge vs Potential (E) (Panel A) and State of Discharge (SOD) vs. E (Panel B) based on coulometric analyses of the cyclic voltammetric data in Fig. 2.

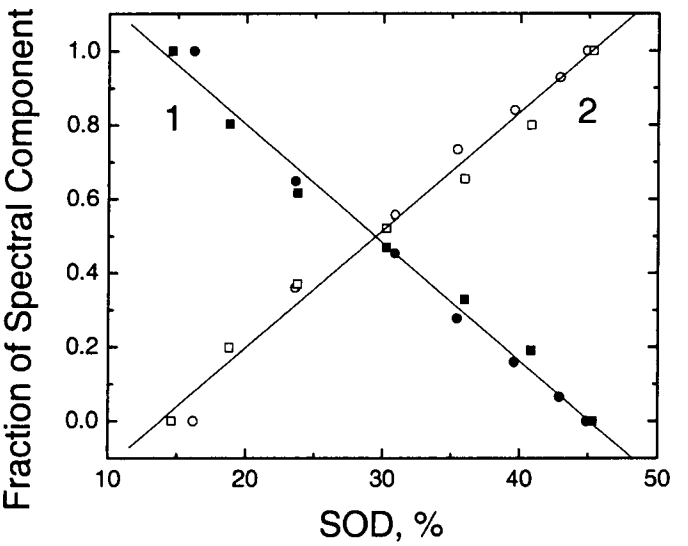


Figure 5. Plots of the fraction of the spectral component for Phase 1 (solid symbols) and Phase (open symbols) for data collected during the scan in the negative (circles) and positive (squares) scans based on a statistical analysis of the spectra shown in thick lines in Fig. 4. The sum of the contributions of each of the two spectrally determined phases to the total Raman spectra was 1 ± 0.02, whereas the linear fits to the data yielded R values larger than 99%.

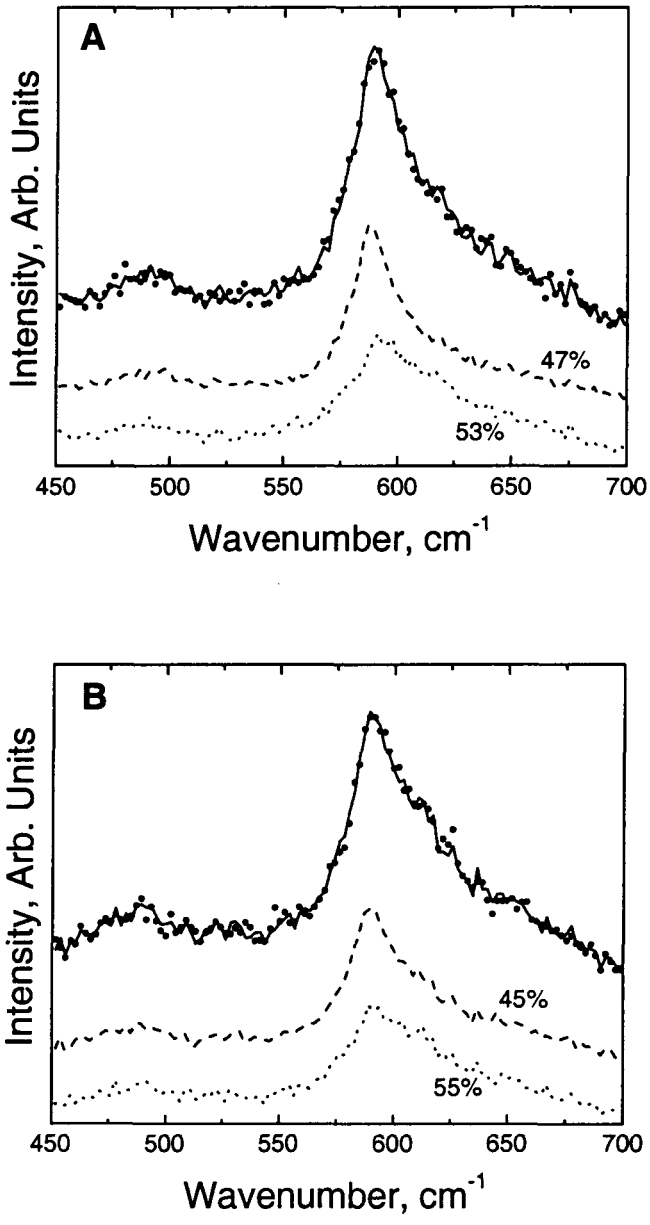


Figure 6. Detailed statistical fits (see solid line through to the actual experimental Raman spectra in scattered points in the upper curves in each Panel) to the Raman data collected at 4.151 V during the positive scan (Panel A) and 4.097 V during the negative scan (Panel B). The bottom curves in each of the panels represent *to scale* the individual contributions from the two pure phases, i.e. SOD = 16 % (E = 4.166 V) for Phase 1, and SOD = 45 % (E = 4.126 V) for Phase 2 in Panel A, and SOD = 16 % (E = 4.118) V for Phase 1, and SOD = 43 % (E = 4.077 V) for Phase 2 in Panel B. The values adjacent to each of the lower curves in Panels A and B correspond to the best-fit percents of each of the phases at the specified potential.